Article:

Yu, Y., Krynkin, A. orcid.org/0000-0002-8495-691X and Horoshenkov, K.V. (2024) The effect of 3D surface roughness on acoustic wave propagation in a cylindrical waveguide. Wave Motion, 128. 103304. ISSN 0165-2125

https://doi.org/10.1016/j.wavemoti.2024.103304

The effect of 3D surface roughness on acoustic wave propagation in a cylindrical waveguide

Yicheng Yu*, Anton Krynkin, Kirill V. Horoshenkov

Department of Mechanical Engineering, University of Sheffield, Mappin Street, Sheffield S1 3JD, UK.

* Corresponding author. E-mail address: Yicheng.Yu@sheffield.ac.uk

Keywords: roughness, pipe, small perturbation method, dispersive curve, sound scattering

Abstract

This paper studies the acoustic wave scattering and attenuation in a cylindrical waveguide with wall roughness varying along all three dimensions and roughness height smaller than the acoustic wavelength. Using the decomposition of the acoustic wave field into deterministic and random components, small perturbation method and Fourier transform the analytical solution of a 3-D averaged acoustic wave field is obtained. The correction term describing the mechanism of wave attenuation caused by roughness and determined by the modal cross-talk is also derived. The solution for the plane wave is validated in the frequency range extended well beyond the second cut-off frequency, where the crosstalk between the fundamental and non-axisymmetric modes are observed. The analytical solution is compared with the numerical results obtained with the Monte-Carlo method and Finite Element solver. The numerical study results have demonstrated a close agreement with the analytical solution for the averaged sound field, dispersion curves, and the wave attenuation effect expressed as the wavenumber correction term. A key novelty of this work is a comprehensive analysis of wave dispersion and cut-off frequency changes due to the presence of 3-D wall roughness.

I. Introduction

The impact of boundary randomness on wave behaviour holds paramount importance in both physical and mathematical contexts, particularly with regards to non-dispersive and dispersive waves, such as those exhibited by seismic, electromagnetic, acoustic, and water waves [1]. Wall roughness effects on the acoustic wave propagation has been studied extensively going back to the Lord Rayleigh's work [2] on wave scattering by a small (compared to the wavelength) periodic grating. The small perturbation method (SPM) was developed [2] and then extensively applied in other research on random rough surfaces (e.g. roughness effects on acoustic scattering [3] and electromagnetic scattering [4]). Another classical method for the analysis of the surface roughness effect is the Kirchhoff Approximation (KA) that assumes that the local wave field is the sum of the incident field and field reflected by the local tangential plane [5, 6]. A more detailed overview of the SPM and KA methods is provided by Ogilvy [7]. Other related methods e.g. small slope approximation [8] and parabolic equation [9], are reviewed by more recent authors [10, 11].

Wall roughness effects in a multimodal acoustic waveguide can be complicated and challenging to predict. For a relatively small wall roughness (compared to acoustic wavelength) the SPM can be used effectively to analyse the random wave field. For example, Bass et al [12] investigated the average field in a statistically irregular waveguide using SPM and Green's function method. Maximov et al [13] applied SPM to study the attenuation and scattering of axisymmetric modes in a fluid-filled round pipe with internally rough walls, where the averaged scattered filed and dispersion relations are presented. A mode coupling solution can also be obtained using SPM as discussed by Brasier et al [14]. Maradudin et al [15] used small perturbation method to predict the attenuation coefficient of Rayleigh waves on flat surfaces due to surface roughness. Krynkin et al [16] used the perturbation method and Fourier analysis to derive the approximation of attenuation of the propagating mode in a 2-D rough waveguide. The approximation proposed in [16] has been applied to analyse the wave scattering due to dynamically rough surface of the turbulent flow in a partially filled circular pipe [17]. Apart from the research work in acoustic wave, perturbation technique has also been used to study water waves (e.g. Ref. [1]) to show that random component in the scattered wave field contributed a linear term with complex coefficient to an evolution equation in a nonlinear context.

Little research has been done to study the separate effects of the axial and circumferential random roughness patterns on the wall of a round pipe, i.e. acoustic wave propagation in a waveguide with the wall roughness varied along all the three dimensions. This pattern of roughness is of particular interest when acoustic waves are used for sensing and communication in pipes which are air-filled (drainage pipes) or pipes partially filled with water, e.g. in sewers [18]. The presence of autonomous robot [19] [20] [21] provides the possibility and capability of carrying the acoustic sensors for the quantification of surface roughness for condition monitoring and maintenance in pipes.

In this paper, SPM and stochastic approach [16] is applied to a 3-D cylindrical waveguide model to account for both the axial and angular patterns in the wall roughness. The plane wave analysis in the previous study (Ref. [16]) was presented as an example in the frequency range below the first cut-off frequency. The small roughness induces the acoustic wave attenuation along the axial direction of the pipe, which may not be observable/measurable below the cut-off frequency with a relatively short propagation distance (<10% amplitude attenuation after travelling distance at 50 times radius of the pipe). To the best of our knowledge, the wave dispersion changes due to the scattering from surface roughness have never been studied analytically in a cylindrical acoustic waveguide. The main novelty of this paper is: (i) derivation of the correction term explaining the shift in the cut-off frequencies and the wave dispersion curves due to the roughness; (ii) the analytical expression predicting both forwards and backwards waves propagating in the pipe with rough walls; (iii) analytical and numerical analysis of the plane wave in the frequency range extended beyond the first/second cut-off frequencies demonstrating the cross-modal effects caused by roughness.

This paper is organised as follows. Section II derives the analytical approximation for the eigen-value problem of a cylindrical pipe with Gaussian roughness wall. This includes Section IIA, where roughness is assumed to be small compared to the wavelength, and the scattered wave field is composed of deterministic (averaged) and random components. In Section IIB, the random and averaged solutions are defined at the waveguide wall by using the Neumann boundary conditions. In Section IIC, the perturbed Helmholtz equation and boundary conditions are solved to predict the eigen-values. Fourier transform is used in the axial domain to account for the statistical properties of the wall roughness. Section IID, discusses the eigen-value correction for plane wave mode in the frequency below the first eigen-frequency. Sections IIE and IIF are used to extend the frequency range to the second and third eigen-frequency, respectively. Section III assesses the analytical model using the Finite Element Method (FEM) validation. The wave scattering effect is presented using the wave dispersion plot in Section IIIA. The wave attenuation of the average plane wave field is discussed in Section IIIB where the numerical method using a finite element model (FEM) is compared with the analytical model. Section IIIC provides the correction term results of the wavenumber of plane wave mode from analytical and numerical predictions.

II. Approximations

The acoustic field in a cylindrical pipe with radius R is the solution of the wave equation written in cylindrical coordinates (r, θ, z). A cylindrical pipe with rough surface, cylindrical coordinate system and the axes orientation are illustrated in Figure 1. Assuming that these waves are propagating in a motionless acoustic medium with density ρ and speed of sound c, the Helmholtz equation is:

$$\Delta p + k^2 p = 0, \tag{1}$$

where $\Delta = \frac{1}{r}\frac{\partial}{\partial r}\left(r\frac{\partial}{\partial r}\right) + \frac{1}{r^2}\frac{\partial^2}{\partial \theta^2} + \frac{\partial^2}{\partial z^2}$ is the Laplacian operator in cylindrical coordinates, $k = \omega/c$ is the acoustic wavenumber in the free field, ω is the angular frequency and p is the frequency dependent sound pressure in the pipe. Note that the time harmonic dependence $\exp(-i\omega t)$ is assumed throughout the paper.

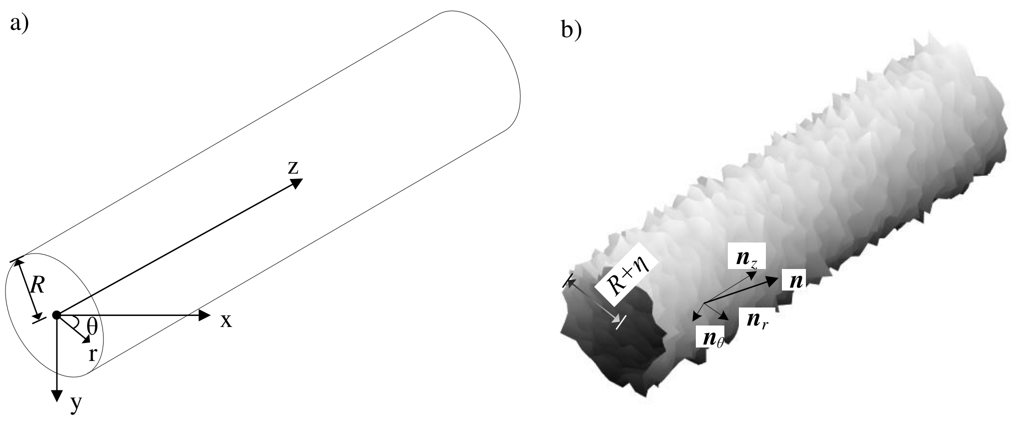

Figure 1. Cylindrical pipe with (a) smooth and (b) rough surface, η denotes the rough surface

Assuming that the stochastically rough surface of the pipe wall can be described by a dual-variable real roughness elevation function $\eta(\theta, z)$ (see Figure 1b), which belongs to the sample space described by the Gaussian distribution with standard deviation σ and correlation length *l.* Gaussian distribution assumption for the rough wall in pipes has been studied and applied extensively e.g. [22] and observed naturally for real surfaces, e.g. [23, 24]. The mean value of $\eta(\theta, z)$ is set to zero which can be expressed as the first moment of the given probability distribution [16]:

$$\bar{\eta}(\theta, z) = \int_{-\infty}^{\infty} \eta(\theta, z) w(\eta, \theta, z)\, d\eta = 0, \tag{2}$$

where $w(\eta, \theta, z)$ is the probability density function of the randomly rough surface.

Random rough surfaces are also characterised by spatial correlation. This can be understood intuitively that at any arbitrary position of the rough pipe surface patterns are related within the correlation radius and become independent at distance bigger than the correlation length. The second moment of the probability distribution that is defined by the dimensionless correlation function:

$$\begin{aligned} W(\theta_1, \theta_2, z_1, z_2) &= \overline{\eta(\theta_1, z_1)\eta(\theta_2, z_2)} \\ &= \int_{-\infty}^{\infty} \eta(\theta_1, z_1)\eta(\theta_2, z_2) w(\eta_1, \theta_1, z_1; \eta_2, \theta_2, z_2)\, d\eta_1 d\eta_2, \end{aligned} \tag{3}$$

with $\lim_{|z_1 - z_2| \to \infty} W(\theta_1, \theta_2, z_1, z_2) = 0$.

The Neumann boundary conditions are imposed on the waveguides wall, yielding [25]:

$$(\boldsymbol{n} \cdot \boldsymbol{\nabla}) p = 0, \tag{4}$$

where $\boldsymbol{n} = n_r \boldsymbol{r} + n_\theta \boldsymbol{\theta} + n_z \boldsymbol{z}$ denotes the unit normal vector to the surface (see Figure 1b), $\boldsymbol{r}$, $\boldsymbol{\theta}$, $\boldsymbol{z}$ are the base unit vectors of cylindrical coordinates, and $\boldsymbol{\nabla} = \left(\frac{\partial}{\partial r}, \frac{\partial}{r\partial \theta}, \frac{\partial}{\partial z}\right)$ is the gradient in cylindrical coordinates. It is assumed here that the rigid pipe is filled with gas (e.g. air) with the characteristic acoustic impedance much smaller than that of the pipe wall. For example, the characteristic acoustic impedance of air is 1.29 kg/m × 343 m/s. It is almost 4 orders of magnitude smaller than the characteristic impedance of a PVC pipe 1330 kg/m^3 × 2400 m/s. The vector $\boldsymbol{n}$ (see Figure 1b) defined in the boundary conditions Eq. (4) can be expressed as:

$$\boldsymbol{n} = \frac{1}{\sqrt{\frac{\eta_\theta^2}{r^2}+1}\sqrt{\eta_z^2+1}}\boldsymbol{r} + \frac{-\frac{\eta_\theta}{r}}{\sqrt{\frac{\eta_\theta^2}{r^2}+1}\sqrt{\eta_z^2+1}}\boldsymbol{\theta} + \frac{-\eta_z}{\sqrt{\eta_z^2+1}}\boldsymbol{z}, \tag{5}$$

where $\eta_\theta = \partial\eta/\partial\theta\,, \eta_z = \partial\eta/\partial z$.

Therefore, the boundary condition on the pipe wall (Eq. (4)) can be expressed as:

$$\left(\frac{1}{\sqrt{\frac{\eta_\theta^2}{r^2}+1}\sqrt{\eta_z^2+1}}\frac{\partial}{\partial r} - \frac{\frac{\eta_\theta}{r}}{\sqrt{\frac{\eta_\theta^2}{r^2}+1}\sqrt{\eta_z^2+1}}\frac{\partial}{r\partial\theta} - \frac{\eta_z}{\sqrt{\eta_z^2+1}}\frac{\partial}{\partial z}\right)p = 0. \tag{6}$$

A. Deterministic and random wave fields

The presence of a stochastically rough wall in the waveguide generates random components in the wave solution of Eq. (1). Therefore, it is assumed that the solution can be decomposed into the averaged p_a and random p_r components [16]:

$$p = p_a + p_r. \tag{7}$$

Note that the statistical averaging of the solution p gives $\bar{p} = p_a$ and $\overline{p_r} = 0$.

The Helmholtz equation (Eq. (1)) for sound field in the pipe with a randomly rough wall can be written as:

$$\left[\frac{1}{r}\frac{\partial}{\partial r}\left(r\frac{\partial}{\partial r}\right) + \frac{1}{r^2}\frac{\partial^2}{\partial\theta^2} + \frac{\partial^2}{\partial z^2}\right](p_a + p_r) + k^2(p_a + p_r) = 0. \tag{8}$$

Eq. (8) can be decomposed into two separate equations [16]:

$$\left[\frac{1}{r}\frac{\partial}{\partial r}\left(r\frac{\partial}{\partial r}\right) + \frac{1}{r^2}\frac{\partial^2}{\partial\theta^2} + \frac{\partial^2}{\partial z^2}\right]p_a + k^2 p_a = 0, \tag{9}$$

$$\left[\frac{1}{r}\frac{\partial}{\partial r}\left(r\frac{\partial}{\partial r}\right)+\frac{1}{r^2}\frac{\partial^2}{\partial\theta^2}+\frac{\partial^2}{\partial z^2}\right]p_r+k^2p_r=0. \tag{10}$$

In this paper it is assumed that the standard deviation σ of the surface roughness is much smaller than the radius of the smooth pipe R which is true in most practical cases, e.g. in buried metal, clay and concrete pipes used to convey water. Therefore, a non-dimensional factor [16] can be defined as:

$$\epsilon=\sigma/R\ll 1, \tag{11}$$

with

$$\sigma=\sqrt{\overline{\eta(\theta,z)^2}}. \tag{12}$$

Note that the dimensionless coordinates, wavenumber, sound pressure and wall roughness used in this paper are:

$$r^*=\frac{r}{R},\qquad z^*=\frac{z}{R},\qquad k^*=kR,\qquad p^*=\frac{p}{\rho c^2},\qquad \eta^*=\frac{\eta}{\sigma}. \tag{13}$$

respectively. For the convenience of expressions, the star is omitted in the following narratives of this paper.

In this paper it is also assumed that the standard deviation σ of the surface roughness is relatively smaller than the acoustic wavelength λ, i.e. $\frac{\sigma}{\lambda}\ll 1$. The random component of the sound pressure p_r should be of order ϵ that links it with the first order moment introduced in Eq. (2), i.e. [16]

$$p_a=\mathcal{O}(1), p_r=\mathcal{O}(\epsilon). \tag{14}$$

Due to the scattered wave field in the presence of the rough surface, the averaged solution p_a can be expressed as [16]:

$$p_a=p_a^{(0)}+\epsilon^2p_a^{(2)}+\mathcal{O}(\epsilon^4), \tag{15}$$

where $p_a^{(0)}$ and $p_a^{(2)}$ denote the averaged solution for the smooth pipe and the small perturbation term, respectively. The second order smallness $\epsilon^2 p_a^{(2)}$ is related to the variance of the surface σ^2 and the correlation function (see Eq. (3)). Using Eqs. (7), (14) and (15), the general solution for p can be expressed as [16]:

$$p = p_a^{(0)} + \epsilon p_r^{(1)} + \epsilon^2 p_a^{(2)} + \mathcal{O}(\epsilon^3), \tag{16}$$

where

$$p_a^{(0)} = \mathcal{O}(1), p_r^{(1)} = \mathcal{O}(1), p_a^{(2)} = \mathcal{O}(1). \tag{17}$$

B. Boundary condition

In the vicinity of the rough surface, $r = 1 + \epsilon\eta(\theta, z)$, the general solution for (7) can be approximated as [16]:

$$p(r, \theta, z) = \left[p + \epsilon\eta \frac{\partial}{\partial r} p + \frac{1}{2}\epsilon^2\eta^2 \frac{\partial^2}{\partial^2 r} p + \mathcal{O}(\epsilon^3)\right]_{r=1}, \tag{18}$$

where r runs from the centre of the pipe as shown in Figure 1. Substituting Eqs. (16)-(18) in Eq. (6), the boundary condition can be given by:

$$\left(\frac{1}{\sqrt{\frac{\eta_\theta^2}{r^2} + 1}\sqrt{\eta_z^2 + 1}} \frac{\partial}{\partial r} - \frac{\frac{\eta_\theta}{r}}{\sqrt{\frac{\eta_\theta^2}{r^2} + 1}\sqrt{\eta_z^2 + 1}} \frac{\partial}{r\partial\theta} - \frac{\eta_z}{\sqrt{\eta_z^2 + 1}} \frac{\partial}{\partial z}\right)\left(1 + \epsilon\eta \frac{\partial}{\partial r} + \frac{1}{2}\epsilon^2\eta^2 \frac{\partial^2}{\partial r^2}\right)\left(p_a^{(0)} + \epsilon p_r^{(1)} + \epsilon^2 p_a^{(2)}\right) = 0, \quad \text{for } r = 1. \tag{19}$$

In order to predict the averaged solution $p_a^{(0)}, p_a^{(2)}$ associated with the boundary condition Eq. (19), the statistical averaging is used here (Eq. (2)). Collecting the terms of the same order of magnitude, Eq. (19) can be rewritten as:

$$\epsilon^0: \quad \frac{\partial p_a^{(0)}}{\partial r} = 0, \qquad \text{for } r = 1; \tag{20}$$

$$\epsilon^1: \quad \frac{\partial p_r^{(1)}}{\partial r} = \eta_\theta \frac{\partial p_a^{(0)}}{\partial \theta} + \eta_z \frac{\partial p_a^{(0)}}{\partial z} - \eta \frac{\partial^2 p_a^{(0)}}{\partial r^2}, \qquad \text{for } r = 1; \tag{21}$$

$$\epsilon^2: \quad \frac{\partial p_a^{(2)}}{\partial r} = \eta_\theta \frac{\partial p_r^{(1)}}{\partial \theta} + \eta_z \frac{\partial p_r^{(1)}}{\partial z} - \eta \frac{\partial^2 p_r^{(1)}}{\partial r^2} - \frac{1}{2}\eta^2 \frac{\partial^3 p_a^{(0)}}{\partial r^3}. \qquad \text{for } r = 1. \tag{22}$$

The mixed derivatives $\frac{\partial^2 p_a^{(0)}}{\partial r \partial \theta}$ and $\frac{\partial^2 p_a^{(0)}}{\partial r \partial z}$ are ignored in the derivation of Eqs. (20), (21) and (22) for reasons similar to those described in Ref. [16] (Eqs. 23-25). Compared with the boundary conditions from Ref. [16] (Eqs. 23-25), this paper discusses the 3D boundary condition including the angular term (the first term at the right side of Eqs. (21) and (22)).

C. Modal eigen-values

In order to find the eigen-value solution for the averaging sound pressure, the 2-D Fourier transform is applied in the axial wave propagation direction (z-axis):

$$\hat{F}(r, m, \xi) = \int_{-\infty}^{\infty} \int_0^{2\pi} F(r, \theta, z) e^{-im\theta} d\theta e^{-i\xi z} dz, \tag{23}$$

where ξ is the wavenumber associated with the acoustic wave propagation in the z-direction, the hat symbol ˆ denotes the Fourier transform applied in the following text. The Fourier integration implemented along the z- and θ- axis can be referred to as averaging along the axis and circumference of the pipe. This can be beneficial for the introduction of statistical feature into the solution. Convergence of the Fourier integrals is required before the Fourier transform. In this paper, Gaussian distribution is used for the realization of the surface roughness, resulting in the integrals existence in the sense of probabilistic convergence that corresponds to the decay of the correlation function at infinity [16].

It makes sense to separate the variables in the sound pressure, i.e. $p\,(r, \theta, z) = \mathcal{R}(r)\Theta(\theta)\mathcal{Z}(z)$. The Fourier transformed Helmholtz equation can be simplified to the Bessel equation:

$$\left[\frac{d^2}{dr^2} + \frac{1}{r}\frac{d}{dr} + \left(k_r^2 - \frac{m^2}{r^2}\right)\right] \hat{\mathcal{R}}_a(r) = 0, \tag{24}$$

$$\left[\frac{d^2}{dr^2}+\frac{1}{r}\frac{d}{dr}+\left(k_r^2-\frac{m^2}{r^2}\right)\right]\hat{\mathcal{R}}_r^{(1)}(r)=0, \tag{25}$$

where $k_r^2=k^2-\xi^2$. $\hat{\mathcal{R}}_a(r)$ and $\hat{\mathcal{R}}_r^{(1)}(r)$ are associated with the radial components of the sound pressure $\hat{p}_a$ and $\hat{p}_r^{(1)}$, respectively. It is assumed that the Fourier parameter ξ is the perturbed eigen-value ξ_{mn} of mode (*m*, *n*) $(m,n\in\mathbb{Z})$ in the pipe with the smooth wall:

$$\xi=\xi_{mn}+\epsilon^2\xi_{mn,2}+O(\epsilon^4)\ \text{ and }\ k_r^2=k_{mn}^2+\epsilon^2k_{mn,2}^2+O(\epsilon^4), \tag{26}$$

where $k_{mn,2}^2=-2\xi_{mn,2}\xi_{mn}$ and $k_{mn}^2=k^2-\xi_{mn}^2$, k_{mn} is the n^{th} root of $\dot{J}_m(k)=0$, which stands for the cross-sectional eigen-value of mode (*m, n*) of the pipe with a smooth wall. On the contrary, the Fourier parameter in Eq. (25) can take any value along the integration path of real axis.

Substituting the expansion of Eq. (26) into Eq. (24), and collecting the same order terms in averaged Eq. (24) gives:

$$\left[\frac{d^2}{dr^2}+\frac{1}{r}\frac{d}{dr}+\left(k_{mn}^2-\frac{m^2}{r^2}\right)\right]\hat{\mathcal{R}}_a^{(0)}=0, \tag{27}$$

$$\left[\frac{d^2}{dr^2}+\frac{1}{r}\frac{d}{dr}+\left(k_{mn}^2-\frac{m^2}{r^2}\right)\right]\hat{\mathcal{R}}_a^{(2)}=-k_{mn,2}^2\hat{\mathcal{R}}_a^{(0)}. \tag{28}$$

Using the Fourier transform, the boundary conditions (Eqs. (20)(21)(22)) can be rewritten as:

$$\epsilon^0:\ \frac{\partial\hat{p}_a^{(0)}}{\partial r}=0, \qquad \text{for } r=1; \tag{29}$$

$$\epsilon^1:\ \frac{\partial\hat{p}_r^{(1)}}{\partial r}=\int_{-\infty}^{\infty}\int_0^{2\pi}\left(\eta_\theta\frac{\partial}{\partial\theta}+\eta_z\frac{\partial}{\partial z}-\eta\frac{\partial^2}{\partial r^2}\right)p_a^{(0)}e^{-im\theta}d\theta e^{-i\xi z}dz,\ \ \text{for } r=1; \tag{30}$$

$$\begin{aligned}\epsilon^2:\ \frac{\partial\hat{p}_a^{(2)}}{\partial r}=\int_{-\infty}^{\infty}\int_0^{2\pi}\Bigg[&\left(\eta_\theta\frac{\partial}{\partial\theta}+\eta_z\frac{\partial}{\partial z}-\eta\frac{\partial^2}{\partial r^2}\right)p_r^{(1)}\\ &-\frac{1}{2}\eta^2\frac{\partial^3}{\partial r^3}p_a^{(0)}\Bigg]e^{-im\theta}d\theta e^{-i\xi z}dz,\ \text{for } r=1.\end{aligned} \tag{31}$$

Using the boundary condition (Eq. (29)) and the Bessel differential equation (Eq. (27)), the unperturbed solution $\hat{p}_a^{(0)}$ for mode (*m, n*) can be given as [25]:

$$\hat{p}_a^{(0)}(r, m, \xi_{mn}) = A_{mn} J_m(k_{mn} r), \tag{32}$$

where $\xi_{mn} = \sqrt{k^2 - k_{mn}^2}$, $m, n \in \mathbb{Z}$, A_{mn} is the modal amplitude which corresponds to the acoustic excitation with a particular source.

Using the deterministic eigen-value from Eq. (26), the leading order averaged solution can be represented by:

$$p_a^{(0)} = \frac{1}{2\pi} \int_{-\infty}^{\infty} \delta(\xi_{mn} - \xi) \hat{p}_a^{(0)}(r, m, \xi) e^{i\xi z} d\xi. \tag{33}$$

The inverse Fourier transform can also be applied to the random component $p_r^{(1)}$ which can be expressed as:

$$p_r^{(1)} = \frac{1}{2\pi} \int_{-\infty}^{\infty} \hat{p}_r^{(1)}(r, m, \xi) e^{i\xi z} d\xi. \tag{34}$$

Substituting Eqs. (33)-(34) into Eqs. (30)-(31), respectively, the boundary conditions (30)-(31) can be rewritten as:

$$\frac{\partial \hat{p}_r^{(1)}}{\partial r} = \int_{-\infty}^{\infty} \delta_R \delta(\xi_{mn} - \xi') \hat{E}(\xi', \tilde{\xi}) \hat{p}_a^{(0)}(r, m, \xi') d\xi', \qquad \text{for } r = 1; \tag{35}$$

$$\frac{\partial \hat{p}_a^{(2)}}{\partial r} = \frac{1}{2\pi} \int_{-\infty}^{\infty} \hat{E}(\xi', \tilde{\xi}) \hat{p}_1^{(1)}(r, m, \xi') d\xi', \qquad \text{for } r = 1. \tag{36}$$

where

$$\hat{E}(\xi', \tilde{\xi}) = \int_{-\infty}^{\infty} \int_0^{2\pi} \left[i m' \eta_\theta + i \xi' \eta_z - \frac{\eta {k_r'}^2 \ddot{J}_{m'}(k_r')}{J_{m'}(k_r')} - \frac{\eta^2 k_{m'n}^3 \dddot{J}_{m'}(k_{m'n})}{2 J_{m'}(k_r')} \right] e^{-im'\theta} d\theta e^{-i\tilde{\xi} z} dz, \tag{37}$$

with $\tilde{\xi} = \xi - \xi'$ and ${k_r'}^2 = \sqrt{k^2 - {\xi'}^2}$, $\ddot{J}_m(\cdot)$ denotes the second order derivative of the *m*th order Bessel function, $\dddot{J}_m(\cdot)$ denotes the second order derivative of the *m*th order Bessel function. The prime mark $(\cdot)'$ for m', ξ', and k_r' is used as a distinctive variable for m, ξ and k_r, respectively. Note that *r* is ignored in $\hat{E}(\xi', \tilde{\xi})$ because the boundary condition is valid when *r*=1. Then the random solution

$\hat{p}_r^{(1)}$ for mode (m, n) can be obtained from Eqs. (25), (35) and (37) using the deterministic leading order solution Eq. (32):

$$\hat{p}_r^{(1)} = B_{mn} J_m(k_r r), \tag{38}$$

with

$$B_{mn} = \frac{\hat{E}(\xi_{mn}, \tilde{\xi}_{mn}) \hat{p}_a^{(0)}(1, m, \xi)}{k_r \dot{J}_m(k_r)}, \tag{39}$$

where $\tilde{\xi}_{mn} = \xi - \xi_{mn}$, $\dot{J}_m(\cdot)$ denotes the first order derivative of the Bessel function. The scattered solution $\hat{p}_a^{(2)}$ can be derived from Eqs. (28) and (36). The Bessel equation (Eq. (28)) is inhomogeneous and this inhomogeneous equation can be generalised as:

$$\left[\frac{d^2}{dx^2} + \frac{1}{x}\frac{d}{dx} + \left(1 - \frac{m^2}{x^2}\right)\right] f_m(x) = -J_m(x). \tag{40}$$

The solution of the above equation $f_m(x)$ can be obtained numerically using Runge-Kutta method [26] (e.g. function @ode45 from Matlab). Here x is a generalized symbol for the inhomogeneous Bessel equation Eq. (40). An example of $f_0(x)$, $f_1(x)$ and their first derivatives is shown in Figure 2.

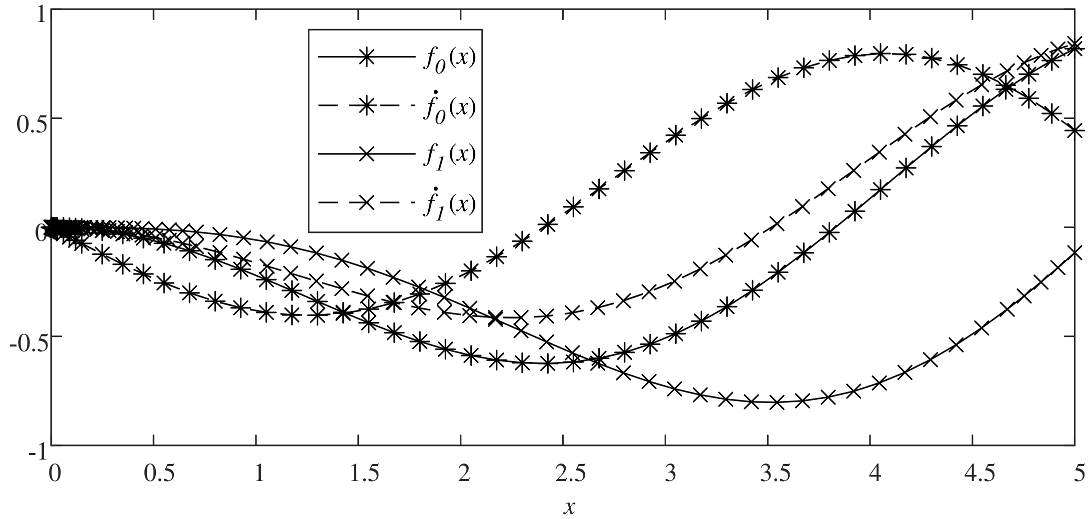

Figure 2. Examples of $f_0(x)$ and $f_1(x)$ and their first derivatives $\dot{f}_0(x)$ and $\dot{f}_1(x)$, respectively.

The solution $\hat{p}_a^{(2)}$ for mode (m, n) from Eq. (28) can then be written as:

$$\hat{p}_a^{(2)} = \frac{A_{mn} k_{mn,2}^2}{k_{mn}^2} f_m(k_{mn} r). \tag{41}$$

The secondary solution of the eigen-value can be obtained by substituting Eq. (38) and (41) into the boundary condition given by Eq. (36):

$$\xi_{mn,2} = -\frac{k_{mn} J_m(k_{mn}) \delta_R I_{mn}}{2\pi \xi_{mn} \dot{f}_m(k_{mn}) \left(1 + \delta_{m0,n0}\right)}, \tag{42}$$

where

$$I_{mn} = \int_{-\infty}^{\infty} \overline{\hat{E}(\xi', \xi_{mn} - \xi') \hat{E}(\xi_{mn}, \xi' - \xi_{mn})} \frac{J_{m'}(k_r')}{k_r' \dot{J}_{m'}(k_r')} d\xi', \tag{43}$$

and

$$\begin{aligned} &\hat{E}(\xi', \xi_{mn} - \xi') \hat{E}(\xi_{mn}, \xi' - \xi_{mn}) \\ &= \iint_{-\infty}^{\infty} \iint_{0}^{2\pi} \left(i m' \eta_{\theta_1} + i \xi' \eta_{z_1} + \alpha {k_r'}^2 \eta_1 + \beta \eta_1^2 k_{m'n}^3\right) \left(i m \eta_{\theta_2} + i \xi' \eta_{z_2} + \alpha_{mn} k_{mn}^2 \eta_2 \right. \\ &\quad \left. + \beta_{mn} \eta_2^2 k_{mn}^3\right) e^{-i\left[(\xi_{mn} - \xi')(z_1 - z_2) + (m - m')(\theta_1 - \theta_2)\right]} d\theta_1 d\theta_2 dz_1 dz_2, \end{aligned} \tag{44}$$

where $\alpha = -\ddot{J}_{m'}(k_r')/J_{m'}(k_r')$, $\alpha_{mn} = -\frac{\ddot{J}_{m'}(k_{mn})}{J_m(k_{mn})}$, $\beta = -\dddot{J}_{m'}(k_r')/2J_{m'}(k_r')$, $\beta_{mn} = -\dddot{J}_m(k_{mn})/2J_m(k_{mn})$.

For a statistically homogeneous wall roughness, the correlation function has the following property $W(x_1, x_2; y_1, y_2) = W(x, y)$ with $x = x_1 - x_2; y = y_1 - y_2$(see Eq. (3)). Therefore, the derivatives of the correlation function with respect to x_1, x_2, y_1, y_2 can be replaced with:

$$\begin{aligned} \overline{\eta_{x_1} \eta_{x_2}} &= -\frac{\partial^2 W(x, y)}{\partial x^2} = -W_{xx}, \\ \overline{\eta_{x_1} \eta(x_2)} &= \frac{\partial W(x, y)}{\partial x} = W_x, \\ \overline{\eta(x_1) \eta_{x_2}} &= -\frac{\partial W(x, y)}{\partial x} = -W_x, \\ \overline{\eta_{x_1} \eta_{y_2}} &= -\frac{\partial^2 W(x, y)}{\partial x \partial y} = -W_{xy}. \end{aligned} \tag{45}$$

Hence, the integration of Eq. (44) can be expressed as:

$$\begin{aligned}
&\overline{\hat{E}(\xi',\xi_{mn}-\xi')\hat{E}(\xi_{mn},\xi'-\xi_{mn})} \\
&= \frac{1}{\delta_R}\left(-m'm+m'^2-\xi'\xi_{mn}+\xi'^2+\alpha k^2-\alpha\xi'^2\right)(-m'm+m^2-\xi'\xi_{mn}+\xi_{mn}^2 \\
&\quad +\alpha_{mn}k^2-\alpha_{mn}\xi_{mn}^2)\widehat{W}(m-m',\xi_{mn}-\xi') \\
&\quad +\beta\beta_{mn}\left(k^2-\xi'^2\right)^{1.5}(k^2-\xi_{mn}^2)^{1.5}\big[1 \\
&\quad +2\widehat{W}^2(m-m',\xi_{mn}-\xi')\big]
\end{aligned} \tag{46}$$

where $\widehat{W}(m-m',\xi_{mn}-\xi')=\int_{-\infty}^{\infty}\int_{-\infty}^{\infty}W(\theta,z)e^{-i[(\xi_{mn}-\xi')z+(m-m')\theta]}dzd\theta$. Using the Fourier transform, the second moment of statistical properties of the roughness can be introduced through the correlation function. Both the circumferential, m, and axial, ξ_{mn}, components are included in the correlation function, $\widehat{W}(m,\xi_{mn})$.

Before solving the wavenumber correction term in Eq. (42), the integral of Eq. (43) can be obtained using the residue theorem. The integrand function is analytic everywhere except at the poles:

$$\xi'=\xi_{qs}^{\pm}=\pm\sqrt{k^2-k_{qs}^2}, \tag{47}$$

where index (q, s) are mode numbers, ξ_{qs} is the axial wavenumber of a smooth waveguide associated with the mode (q, s). The sign $\pm$ is the direction of the wavenumber which means that the scattered wave can propagate forwards or backwards in the waveguide. Since (q, s) is not necessarily the same as (m, n), this introduces the cross-mode effects (modal crosstalk). According to Eq. (47), the integral is only calculated at the poles equal to the eigen-values, which means only the wavenumbers at eigen-values are effective. The phenomenon implies that the rough surface can be effectively replaced by extraneous sources distributed over the waveguide wall that radiates waves propagating with different modes [7].

Using the residue theorem, the integration I_{mn} in Eq. (42) can be rewritten as:

$$I_{mn} = 2\pi i \lim_{\xi' \to \xi_{qs}^{\pm}} \left\{ \frac{J_{m'}\left(k_r'\right)\left(\xi' - \xi_{qs}^{\pm}\right)}{k_r' \dot{J}_{m'}\left(k_r'\right)} \left(-m'm + m'^2 - \xi'\xi_{mn} + \xi'^2 + \alpha k^2 - \alpha \xi'^2 \right) \left(-m'm + m^2 - \xi'\xi_{mn} + \xi_{mn}^2 + \alpha_{mn}k^2 - \alpha_{mn}\xi_{mn}^2 \right) \widehat{W}\left(m, \xi_{mn} - \xi'\right) + \beta\beta_{mn}\left(k^2 - \xi'^2\right)^{1.5}\left(k^2 - \xi_{mn}^2\right)^{1.5}\left[1 + 2\widehat{W}^2\left(m - m', \xi_{mn} - \xi'\right)\right] \right\} \tag{48}$$

$$= 2\pi i \frac{J_q\left(k_{qs}^{\pm}\right)}{\dot{J}_q\left(k_{qs}^{\pm}\right)\xi_{qs}^{\pm}} \left\{ \left(-qm + q^2 - \xi_{qs}^{\pm}\xi_{mn} + {\xi_{qs}^{\pm}}^2 - \frac{\ddot{J}_q\left(k_{qs}^{\pm}\right)}{J_q\left(k_{qs}^{\pm}\right)} {k_{qs}^{\pm}}^2 \right) \left(-qm + m^2 - \xi_{qs}^{\pm}\xi_{mn} + \xi_{mn}^2 - \frac{\ddot{J}_m\left(k_{mn}\right)}{J_m\left(k_{mn}\right)} k_{mn}^2 \right) \widehat{W}\left(m - q, \xi_{mn} - \xi_{qs}^{\pm}\right) + \frac{\dddot{J}_q\left(k_{qs}^{\pm}\right)}{4J_q\left(k_{qs}^{\pm}\right)} \frac{\dddot{J}_m\left(k_{mn}\right)}{J_m\left(k_{mn}\right)} k_{mn}^3 {k_{qs}^{\pm}}^3 \left[1 + 2\widehat{W}^2\left(m - q, \xi_{mn} - \xi_{qs}^{\pm}\right)\right] \right\}.$$

From Eq.(48), the correction term of wavenumber $\xi_{mn,2}$ can be obtained:

$$\xi_{mn,2} = \frac{i}{2} \sum_{q=0}^{Q} \sum_{s=0}^{S} \frac{k_{mn} J_m\left(k_{mn}\right)}{\xi_{mn}\xi_{qs}^{+}\dot{J}_m\left(k_{mn}\right)\left(1 + \delta_{m0,n0,q0,s0}\right)} \frac{J_q\left(k_{qs}\right)}{\dot{J}_q\left(k_{qs}\right)} \left\{ \left(-qm + q^2 - \xi_{qs}^{\pm}\xi_{mn} + {\xi_{qs}^{\pm}}^2 - \frac{\ddot{J}_q\left(k_{qs}^{\pm}\right)}{J_q\left(k_{qs}^{\pm}\right)} {k_{qs}^{\pm}}^2 \right) \left(-qm + m^2 - \xi_{qs}^{\pm}\xi_{mn} + \xi_{mn}^2 - \frac{\ddot{J}_m\left(k_{mn}\right)}{J_m\left(k_{mn}\right)} k_{mn}^2 \right) \widehat{W}\left(m - q, \xi_{mn} - \xi_{qs}^{\pm}\right) + \frac{\dddot{J}_q\left(k_{qs}^{\pm}\right)}{4J_q\left(k_{qs}^{\pm}\right)} \frac{\dddot{J}_m\left(k_{mn}\right)}{J_m\left(k_{mn}\right)} k_{mn}^3 {k_{qs}^{\pm}}^3 \left[1 + 2\widehat{W}^2\left(m - q, \xi_{mn} - \xi_{qs}^{\pm}\right)\right] \right\}. \tag{49}$$

For the full solution for the wavenumber in Eqs. (49), the statistical properties expressed through the correlation function are required. For the dual variable, a 2-D Gaussian correlation function is proposed here for the 3-D modelling:

$$W(\theta,z)=e^{-\frac{z^2+R^2\theta^2}{l^2}}, \tag{50}$$

which can be rewritten in a normalized form:

$$W(\theta,z^*)=e^{-\frac{{z^*}^2+\theta^2}{l^2}}. \tag{51}$$

Note that this 2-D correlation function depends on the distance separation in the axial as well as the circumferential directions. For simplicity, the star sign in Eq. (51) is eliminated throughout the text.

Its Fourier transform can be given by:

$$\widehat{W}(m,\xi)=\sqrt{\pi}le^{-\frac{\xi^2l^2+m^2l^2}{4}}. \tag{52}$$

Therefore, the full equation of the wavenumber (Eq. (26)) can be rewritten as:

$$\begin{aligned}\xi=\xi_{mn}+\frac{i\sigma^2}{2R^2}\sum_{q=0}^{Q}\sum_{s=0}^{S}&\frac{k_{mn}J_m(k_{mn})}{\xi_{mn}\xi_{qs}^{+}\dot{J}_m(k_{mn})(1+\delta_{m0,n0,q0,s0})}\frac{J_q(k_{qs})}{\ddot{J}_q(k_{qs})}\Bigg\{\Bigg(-qm+q^2\\&-\xi_{qs}^{\pm}\xi_{mn}+{\xi_{qs}^{\pm}}^2-\frac{\ddot{J}_q(k_{qs}^{\pm})}{J_q(k_{qs}^{\pm})}{k_{qs}^{\pm}}^2\Bigg)\Bigg(-qm+m^2-\xi_{qs}^{\pm}\xi_{mn}+\xi_{mn}^2\\&-\frac{\ddot{J}_m(k_{mn})}{J_m(k_{mn})}k_{mn}^2\Bigg)\widehat{W}\left(m-q,\xi_{mn}-\xi_{qs}^{\pm}\right)\\&+\frac{\ddot{J}_q(k_{qs}^{\pm})}{4J_q(k_{qs}^{\pm})}\frac{\ddot{J}_m(k_{mn})}{J_m(k_{mn})}k_{mn}^3{k_{qs}^{\pm}}^3\left[1+2\widehat{W}^2\left(m-q,\xi_{mn}-\xi_{qs}^{\pm}\right)\right]\Bigg\}.\end{aligned} \tag{53}$$

Therefore, the wave scattering from the rough surface is dependent on the mode patterns, the cross-correlation and standard deviation of the roughness.

When $k>k_{mn}$, $k>k_{qs}$, the wavenumbers ξ_{mn} and $\xi_{qs}^{\pm}$ are real number, which represents the wave propagation in the smooth pipe in the form of mode (*m, n*) and the scattering wave in the form of mode (*q, s*), respectively. The wavenumber correction term $\xi_{mn,2}$ is imaginary which represents the wave attenuation for the average pressure field.

When $k_{mn}<k<k_{qs}$ (where k is slightly smaller than k_{qs}), which means ξ_{mn} is real and $\xi_{qs}^{\pm}$ is imaginary, corresponding to the wave propagation for the smooth pipe acoustic pressure field at mode (*m, n*) and the evanescent scattering wave at mode (*q, s*), respectively. Here we only discuss the case

that k is slightly smaller than k_{qs}, otherwise the evanescent wave mode (*q*, *s*) attenuates rapidly enough that does not contribute to the wave field and can be truncated by Q, S in the upper limit of the summation in Eq. (53). The wavenumber correction term $\xi_{mn,2}$ is complex with its imaginary part representing the wave attenuation for the averaged pressure field, and its real part representing the wave propagation. This means that the imaginary scattering wavenumber ξ_{qs} corresponding to evanescent modes can transfer energy and contribute to the propagating wave mode (*m*, *n*). Although evanescent waves do not propagate and decay axially, the scattering due to the rough surface continuously generates these evanescent waves all along the pipe contributing to wave propagation. A "propagating" wave can be scattered by the rough surface and generate the propagating wave mode (*m*, *n*). This phenomenon will be discussed in detail in the following section with an example of plane wave mode.

When $k_{qs} < k < k_{mn}$ (where k is slightly smaller than k_{mn}) ξ_{mn} is imaginary and $\xi_{qs}^{\pm}$ is real. These correspond to the evanescent wave for the averaged pressure field at mode (*m*, *n*) and the propagating scattered wave at mode (*q*, *s*), respectively. Again $\xi_{mn,2}$ is complex with its imaginary part representing the wave attenuation for the averaged pressure field, and its real part representing the wave propagation. For $k < k_{mn}$, ξ_{mn} is imaginary corresponding to evanescent wave modes. Although these modes do not propagate in a smooth pipe, they can be scattered continuously along the axial direction by the rough surface and contribute to the propagating wave $\xi_{qs}^{\pm}$. The phenomenon of a non-propagating wave scattered into a propagating wave due to the rough surface results in the reduced cut-off frequency. This will be validated via numerical simulation in Section III.

When $k = k_{mn}, \xi_{mn} = 0$, this means that the wave could not propagate and result in an infinite attenuation. The corrected wavenumber, denoted as $\xi_{mn,2}$, exhibits singularity at this particular frequency ($k = k_{mn}$) due to the presence of ξ_{mn} in the denominator of Eq. (53). This will be discussed more with the numerical validation in Section III.

Note that the wavenumber ξ_{mn} has commutative properties so that mode index pairs (*m*, *n*) and (*q*, *s*) are interchangeable. This means that the propagating wave mode (*m*, *n*) can transfer energy to mode

(q, s) after scattering from the rough surface and vice versa. It should be noted that this paper does not quantify the energy transfer between the cross-mode effects.

In the following section, the fundamental mode (plane wave) will be discussed as an example using the theoretical results from Eq. (53) to illustrate the acoustic wave attenuation in a rough waveguide. Furthermore, this paper will also investigate the plane wave behaviour beyond the first eigen-frequency to illustrate how its propagation is affected by other higher-order modes.

D. Plane wave mode when $f<f_{10}$

In the frequency range where a smooth cylindrical waveguide only supports the plane wave m, n =0, the wavenumber $\xi_{00} = k$, $k_{mn} = 0$, $\lim_{k_{mn}\to 0} \frac{\dot{f}_0(k_{mn})}{k_{mn}} = -0.5$. Therefore, Eq. (49) can be reduced to:

$$\xi_{00,2} = \frac{i\sigma^2}{2R^2} k^2 \widehat{W}(0,2k). \tag{54}$$

Eq. (54) is the result identical to Eq. (50) from Ref. [16]. The averaged acoustic pressure in the cylindrical waveguide with a stochastically rough surface can be approximated by Eqs. (15),(41):

$$p_a = \lim_{k_{00}\to 0} A_{00} \left[1 + \frac{k_{00,2}^2}{k_{00}^2} f_0(k_{00} r)\right] e^{i(k+\xi_{00,2})z}. \tag{55}$$

Using $k_{00,2}^2 = -2\xi_{00,2}\xi_{00}$, $\xi_{00} = k$, $\lim_{x\to 0} \dot{f}_0(x)/x = -0.5$ this equation can be simplified as:

$$\begin{aligned} p_a = A_{00} g(r) e^{i(k+\xi_{00,2})z} \text{ with } g(r) &= 1 - 2k\xi_{00,2} \lim_{k_{00}\to 0} f_0(k_{00} r)/k_{00}^2 \\ &= 1 + \frac{1}{2} k \xi_{00,2} r^2. \end{aligned} \tag{56}$$

Therefore, the acoustic pressure of the averaged field not only attenuates along the axial direction, but also increases with radial direction and reaches the maximum value close to the rough wall.

E. Plane wave mode when $f_{10}<f<f_{20}$

When the frequency range is extended above the first eigen-frequency (f_{10}), the plane wave can be affected by the mode coupling, e.g. the energy from mode (0,0) can leak into mode (1,0) and vice versa because in the frequency range $f_{10}<f<f_{20}$ two different modes (0,0) and (1,0) can propagate. For mode (1,0) the wavenumber of a smooth pipe is $\xi_{10} = \sqrt{k^2 - k_{10}^2}$, $k_{10} = 1.841$ (which can be

obtained from Eq. (29)), Eq. (49) can be reduced to:

$$\xi_{00,2} = \frac{i\sigma^2}{2R^2}\Bigg[k^2\widehat{W}(0,2k) + \frac{J_1(k_{10})}{4k\xi_{10}\dot{J}_1(k_{10})}\left({\xi_{10}}^2 - k\xi_{10} - \frac{\ddot{J}_1(k_{10})}{J_1(k_{10})}\,k_{10}^2\right)(k^2 - k\xi_{10})\widehat{W}(1, k-\xi_{10}) + \frac{J_1(k_{10})}{4k\xi_{10}\dot{J}_1(k_{10})}\left({\xi_{10}}^2 + k\xi_{10} - \frac{\ddot{J}_1(k_{10})}{J_1(k_{10})}\,k_{10}^2\right)(k^2 + k\xi_{10})\widehat{W}(1, k+\xi_{10})\Bigg]. \tag{57}$$

The first term on the right side of Eq. (57) is the plane wave mode solution (see Eq. (54)).

When ξ_{10} is real ($k > k_{10}$), the second term represents the coupling effect between mode (0,0) and mode (1,0) which propagate forward, whereas the third term represents the coupling effect between mode (0,0) and mode (1,0) which propagate backward.

When ξ_{10} is imaginary ($k < k_{10}$, again it is assumed k is slightly smaller than k_{10}), the scattered wave mode is evanescent and decays exponentially in the axial direction. This imaginary wavenumber contributes the real part of the wavenumber $\xi_{00,2}$ in Eq. (57) which represents the propagating wave pattern. The second term of the right side of Eq. (57) was calculated from ξ_{10}^{+} which is associated with the positive (forward) "propagating" evanescent wave, whereas the third term calculated from ξ_{10}^{-} is associated with the negative (backwards) "propagating" evanescent wave.

F. Plane wave mode when $f_{20}<f<f_{01}$

In the frequency range where three modes can propagate along the pipe: i.e. modes (0,0), (1,0), (2,0). The wavenumber for mode (2,0) is $\xi_{20} = \sqrt{k^2 - k_{20}^2}$, $k_{20} = 3.054$ (which can be obtained from Eq. (29)). Therefore, Eq. (49) can be reduced to:

$$\xi_{00,2} = \frac{i\sigma^2}{2R^2}\Bigg[k^2\widehat{W}(0,2k)$$

$$+\frac{J_1(k_{10})}{4k\xi_{10}\ddot{J}_1(k_{10})}\left({\xi_{10}}^2 - k\xi_{10} - \frac{\ddot{J}_1(k_{10})}{J_1(k_{10})}\,k_{10}^2\right)(k^2 - k\xi_{10})\widehat{W}(1,k-\xi_{10})$$

$$+\frac{J_1(k_{10})}{4k\xi_{10}\ddot{J}_1(k_{10})}\left({\xi_{10}}^2 + k\xi_{10} - \frac{\ddot{J}_1(k_{10})}{J_1(k_{10})}\,k_{10}^2\right)(k^2 + k\xi_{10})\widehat{W}(1,k+\xi_{10}) \tag{58}$$

$$+\frac{J_2(k_{20})}{4k\xi_{20}\ddot{J}_2(k_{20})}\left({\xi_{20}}^2 - k\xi_{20} - \frac{\ddot{J}_2(k_{20})}{J_2(k_{20})}\,k_{20}^2\right)(k^2 - k\xi_{20})\widehat{W}(2,k-\xi_{20})$$

$$+\frac{\ddot{J}_2(k_{20})}{4k\xi_{20}J_2(k_{20})}\left({\xi_{20}}^2 + k\xi_{20} - \frac{\ddot{J}_2(k_{20})}{J_2(k_{20})}\,k_{20}^2\right)(k^2 + k\xi_{20})\widehat{W}(2,k+\xi_{20})\Bigg].$$

The second and third terms represent the coupling effect between mode (0,0) and mode (1,0) where mode (1,0) propagates forward and backward, respectively. The fourth and fifth terms represent the coupling effect between mode (0,0) and mode (2,0) where mode (2,0) propagates forward and backward, respectively. Note that the coupling of the scattering wave between mode (1,0) and (2,0) are ignored here since the scattering waves are assumed as a first order small term.

The use of "propagating" evanescent wave discussed in the previous section is also valid here for the second non-axisymmetric mode.

III. Numerical simulation

In this study, a 6m long, 150mm diameter pipe was used to study the 3-D surface roughness effects. The surface roughness matrix was generated by Gaussian distribution function in MATLAB, with zero mean and standard deviation $\frac{\sigma}{R}$. The matrix rows and columns represent the roughness realization in the axial and angular directions, respectively. The number of rows and columns was determined by the spatial separation *d* between random values of the surface. The spatial separation between random numbers defines the effective correlation length $d = \sqrt{\pi}l$ [16]. This surface roughness matrix can be imported to the FEM simulation software using COMSOL as interpolation function. The geometry of the pipe wall with roughness can be generated using the parametric surface characterised by the interpolation function. Figure 1b shows an example of rough surface generated by parametric surface using COMSOL.

A. Surface roughness effects on wave dispersion in an empty pipe

In order to understand better the acoustic pressure distribution along an empty pipe with surface roughness, the wave dispersion was investigated. The dispersion relation of acoustic wave could be determined based on the frequency responses from FEM simulation in COMSOL.

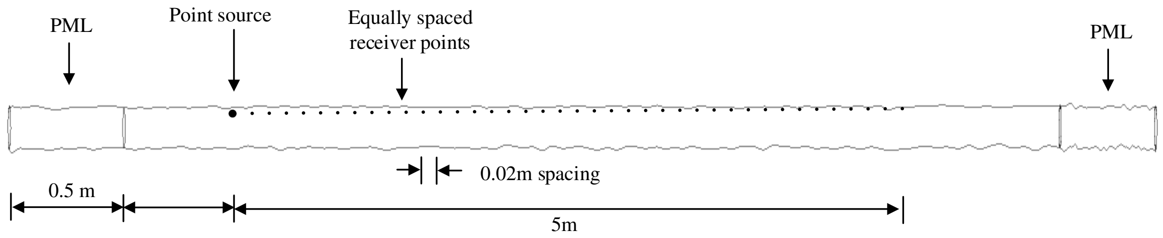

Figure 3. An illustration of the simulation setup for surface roughness effects on wave dispersion with point source excitation.

As shown in Figure 3, a point source was set up close to the pipe wall so that both the anti-axisymmetic and axisymmetric modes could be excited. The receiver points were also located close to the pipe wall to measure different modes. These were located from 20mm to 5m with a 20mm sptial step. The distance and frequency were normalized with respect to the pipe radius to generalize the conclusion for a pipe with an arbitrary radius. Perfectly matched layers (PML) were used at both ends of the pipe to minimise any sound reflections. The tetrahedral elements were used for the mesh of the whole system. The minimum size of the element was 0.0086m, i.e. around 0.1 of the wavelength at 4kHz. This simulation was implemented on a workstation with Intel(R) Core(TM) i7-9800X CPU @ 3.80GHz and 128G RAM, which takes around 5 hours for a computation with 20 Hz frequency step up to 4kHz. Applying the Fourier transform to the spatial domain, the wave dispersion can be obtained with the results shown in Figure 4.

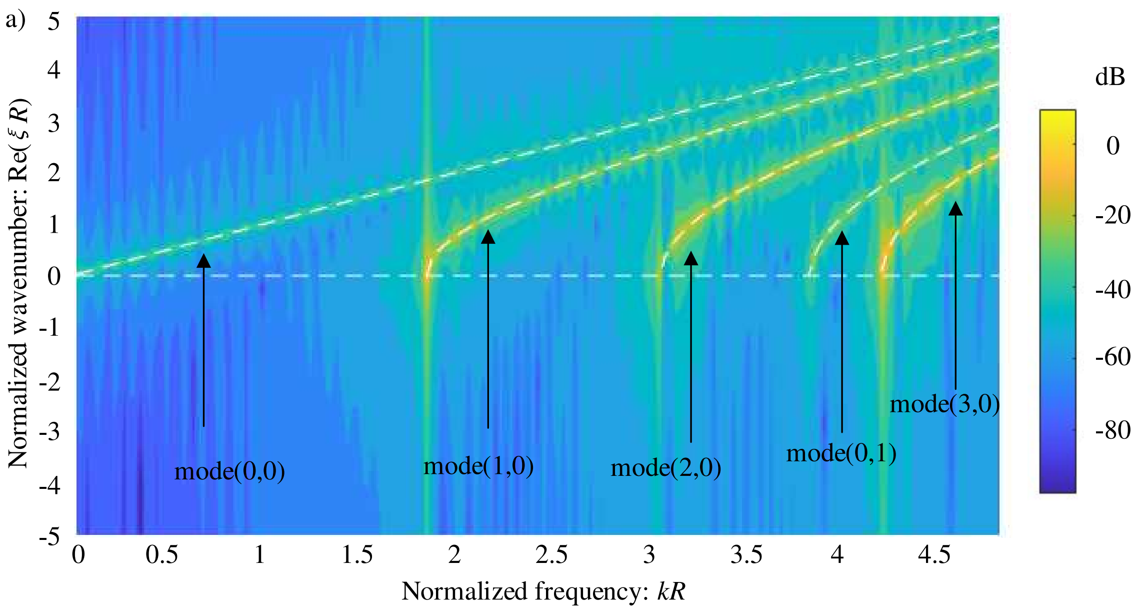
a)
Normalized wavenumber: Re(ξ R)
Normalized frequency: kR
mode(0,0)
mode(1,0)
mode(2,0)
mode(0,1)
mode(3,0)
dB
0
-20
-40
-60
-80

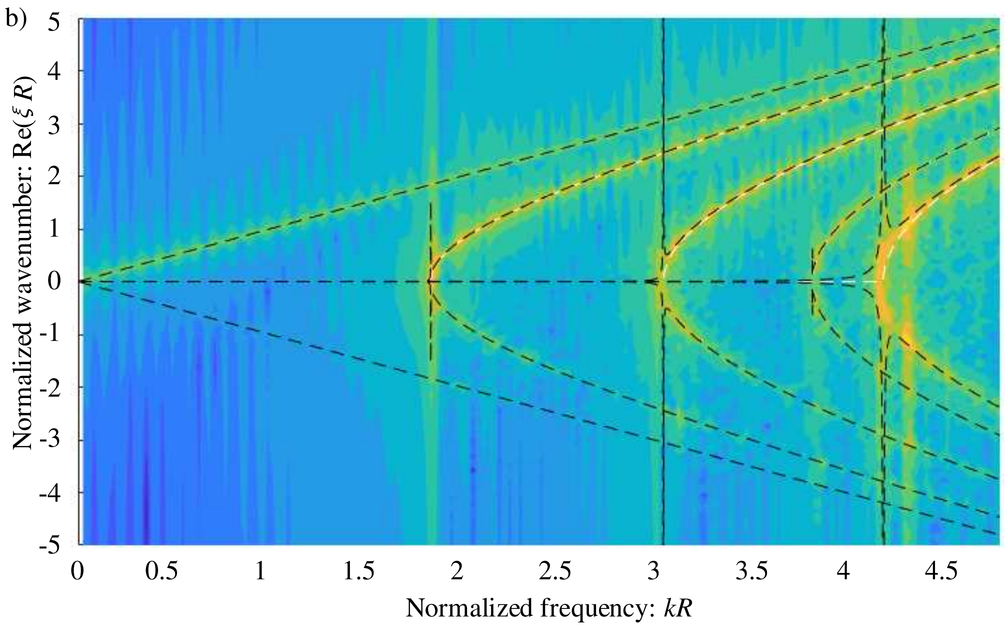
b)
Normalized wavenumber: Re(ξ R)
Normalized frequency: kR

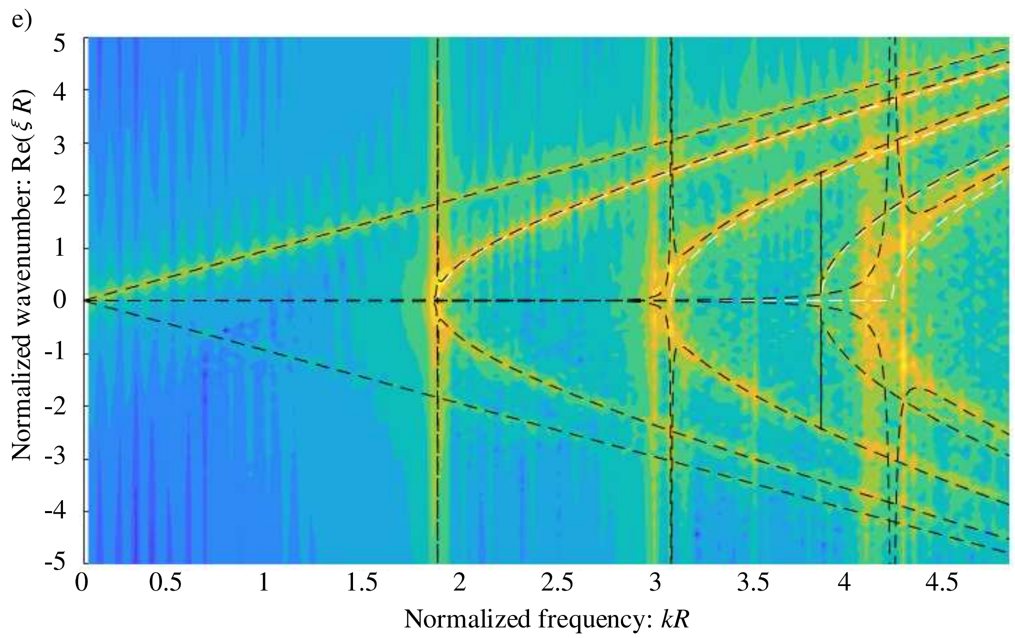

Figure 4. The dispersion relations using a point source excitation in a pipe with: (a) smooth surface, (b) surface roughness ($\sigma/R = 0.05$), (c) surface roughness ($\sigma/R = 0.1$). Colormap: COMSOL simulation; dashed white line: theoretical wave dispersion for the smooth pipe, dashed black line: theoretical wave dispersion using Eq. (53). Colour-bar: normalized amplitude of acoustic pressure level (dB).

As shown in Figure 4a, the simulated dispersive contour plot shows a close agreement of the theoretical solution for an empty smooth pipe. This simulation method was then applied to pipes with rough surfaces with $\sigma/R = 0.05$ and $\sigma/R = 0.1$ as shown in Figure 4b and Figure 4c, respectively. Compared with the smooth pipe, surface roughness results in the negative wavenumber components that represent the scattered wave propagating backwards. As expected, the scattering tends to be more significant when the surface roughness becomes larger. Furthermore, these scattered waves due to the rough surface tend to propagate in the form of the same modes as in the case of the pipe with smooth walls. This provides the same conclusion as discussed in Sec. II. From the theoretical study in Sec. II, Eqs. (47)(48), the scattered wavenumber ξ' is effective only when it is equal to the eigen-modes of a smooth pipe $\xi' = \xi_{qs}^{\pm}$. The wavenumber $\xi_{qs}^{\pm}$ is the axial wavenumber of (q, s) mode of a smooth pipe, and the positive and negative sign of the wavenumber $\xi_{qs}^{\pm}$ denote the wave that propagates forward and backward, respectively. This means that the scattered wave due to the surface roughness propagates as a superposition of modes predicted for a smooth pipe interfering with the deterministic (averaged) propagating wave.

The numerical results show that the cut-off frequency of the first three non-axisymmetric modes reduces relative to the amplitude of the standard deviation of the rough surface, whereas the axisymmetric mode (0, 1) does not exhibit significant changes. This indicates the importance of the contribution from circumferential roughness that highlights the necessity of 3-D modelling.

As discussed in the theoretical study, the reduction of the cut-off frequency and the shift of the dispersion curve is due to the "propagating" evanescent wave. The analytical solution of the dispersion curve shows close agreement with the numerical results, which supports the validity of the analytical solution proposed in the paper. The reduction of the cut-off frequency and the shift of the dispersion curve tend to be more significant with larger standard deviation of the roughness.

As shown in Figure 4b and 4c, the backwards propagating plane wave (negative wavenumber) is generated by the scattering from the rough surface. The amplitude of the scattered plane wave below the first cut-off frequency (kR =1.841) is slightly smaller than the plane wave above the first cut-off frequency (kR =1.841). This is because of the higher modes at frequencies kR>1.841 also contribute to the scattered plane wave, which provides the evidence of the theorical discussion on the cross-mode effects, and this cross-mode effect becomes more significant with larger σ/R by comparing the Figure 4b and 4c.

As shown in Figure 4b and 4c, there are singular points in the dispersion curves of higher modes at the eigen-frequencies of the smooth pipe (when $\xi_{mn} = 0$). This means that the acoustic wave at mode (m, n) is converted into a standing wave.

To explicitly illustrate the cross-mode effect, an example of the acoustic field distribution and wave dispersion only using plane wave background excitation in a pipe with surface roughness ($\sigma/R = 0.1$) is shown in Figure 5. At both ends of the pipe, PMLs were used to absorb the acoustic wave for the assumption of infinitely long pipe. Figure 5a presents an example of the acoustic wave distribution at the frequency kR=1.81 which is slightly smaller than the first cut-ff frequency kR=1.84.

The composite wave field consists of the plane wave mode in conjunction with the "propagating" evanescent first non-axisymmetric mode (1,0), which exhibits a complex wave field. The rotational motion of the first non-axisymmetric mode (1,0) arises from the stochastic scattering occurring at the rough surface, as depicted in Figure 5a. Further insights into the spatial distribution of sound pressure are provided in Figure 5b-d, showcasing a detailed cross-sectional view. The rotational behavior of mode (1,0) is attributed to the presence of double eigenvalues for non-axisymmetric modes, such as (mode (1,0)), with the corresponding eigenfunctions being identical but phase-shifted by 90 degrees. Superimposing these two eigenfunctions obtains acoustic rotational mode patterns (e.g. [27]).

Even though only the plane wave background excitation was used, the energy of the plane wave transferred to the first mode (1,0) as well as other higher modes as shown in the dispersion curve in Figure 5b. The scatted wave field due to the cross-mode effect exhibits close agreement with analytical solution (<10% error apart from at the cut-off frequency of the smooth pipe). Whereas in a smooth pipe, the wave dispersion only exhibits the plane wave without the energy transfer to higher mode as expected (see A1 in the Appendix).

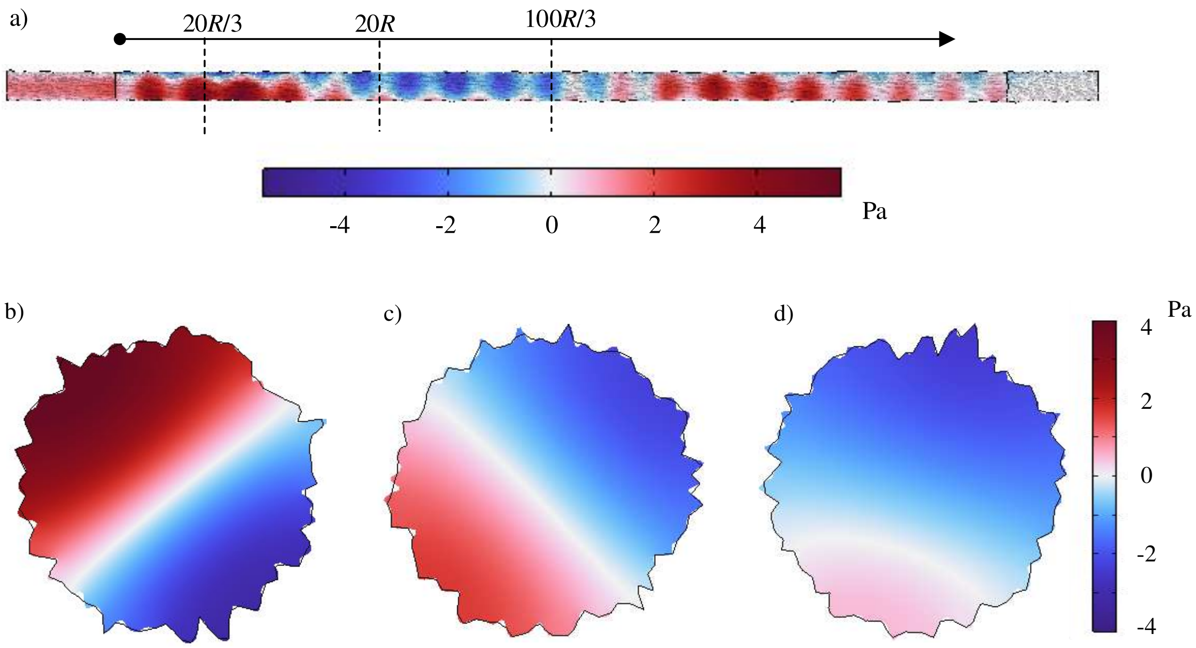

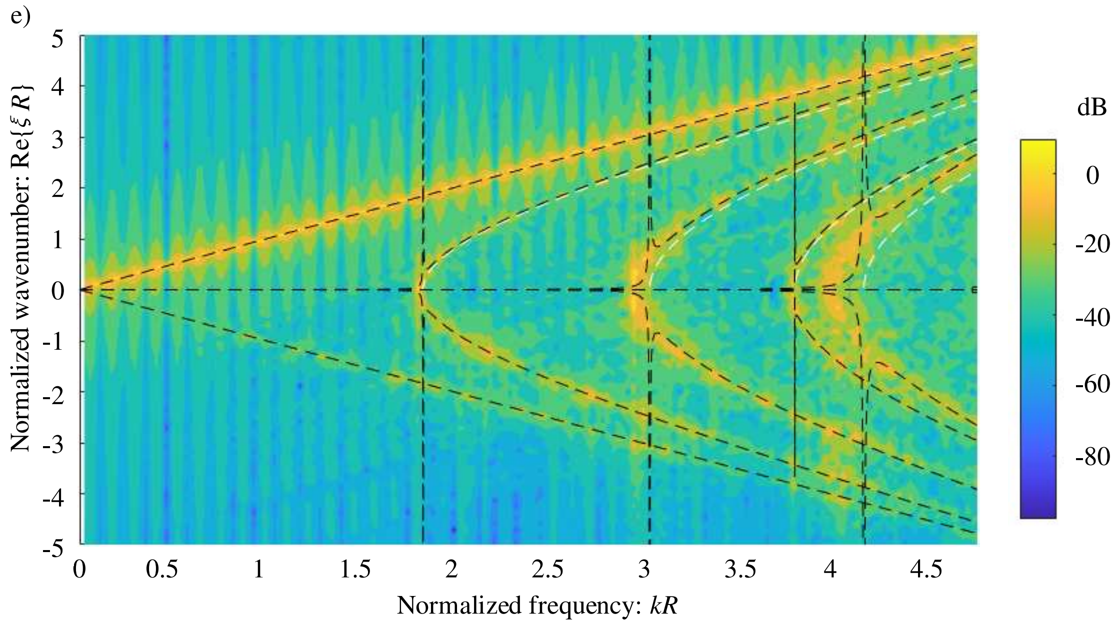

Figure 5. (a) an illustration of the acoustic field distribution (real part of wavenumber) using plane wave background excitation in a pipe with surface roughness ($\sigma/R = 0.1$) at normalized frequency kR=1.81; (b)-(d) the cross section acoustic pressure distribution at axial coordinates 20R/3, 20R, and 100R/3, respectively; (e) the dispersion relations of plane wave background excitation in a pipe with surface roughness ($\sigma/R = 0.1$). Colormap: COMSOL simulation (amplitude of sound pressure); dashed white line: theoretical wave dispersion for the smooth pipe, dashed black line: theoretical wave dispersion using Eq. (53). Colour-bar: normalized amplitude of acoustic pressure level (dB).

B. Surface roughness effects on averaged plane wave field

In this section, the numerical model was implemented using COMSOL with plane wave excitation in a cylindrical pipe with surface roughness defined in the beginning of Section III.

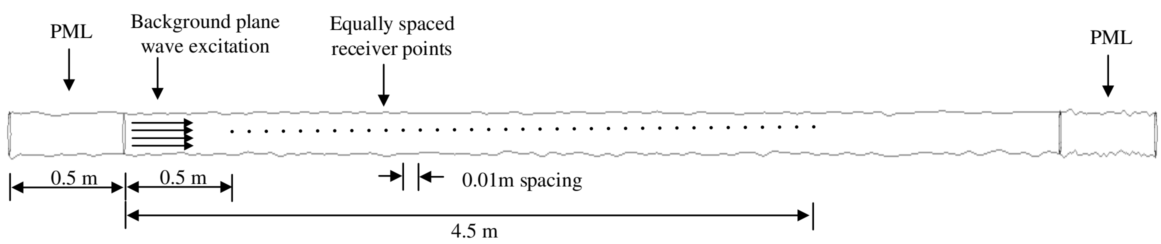

Figure 6. An illustration of the simulation setup for surface roughness effects on wave attenuation with plane wave excitation.

As shown in Figure 3, a point source was applied close to the pipe wall so that both the anti-axisymmetic and axisymmetric modes could be excited. The receiver points were also located close to the pipe wall to measure different modes. These were located from 0.5 m to 4.5 m with a 10mm sptial step. The distance and frequency were normalized with respect to the pipe radius to generalize the conclusion for a pipe with an arbitrary radius. Perfectly matched layers (PML) were used at both ends of the pipe to minimise any sound reflections. The tetrahedral elements were used for the mesh of the whole system. The minimum size of the element is 0.0086m which is around 0.1 times of wavelength at 4k Hz. To obtain the averaged numerical solution for multiple samples of the random surface Monte Carlo method was used with FEM resulting in around 5 hours for each sample to be computed on a workstation with Intel(R) Core(TM) i7-9800X CPU @ 3.80GHz and 128G RAM, which takes around 5 hours for a computation with 20 Hz frequency step up to 4k Hz..

The analytical model proposed in this paper can be used to estimate the averaged wave attenuation in the cylindrical pipes with rough surface. Using the analytical model, the computation cost can be dramatically reduced (the computational cost for a single surface sample of the numerical model is 10^4 times greater than that with the analytical calculations). It is worth noting that a rigorous convergence of the averaged sound pressure in the numerical model requires more than 10^3 realizations [16] which could not be achieved in this paper due to the computationally expensive numerical validation. Instead, 40 samples of the rough surface were used to generate the numerical solution that limits the accuracy of the numerical model but maintains the general trend of the averaged solution.

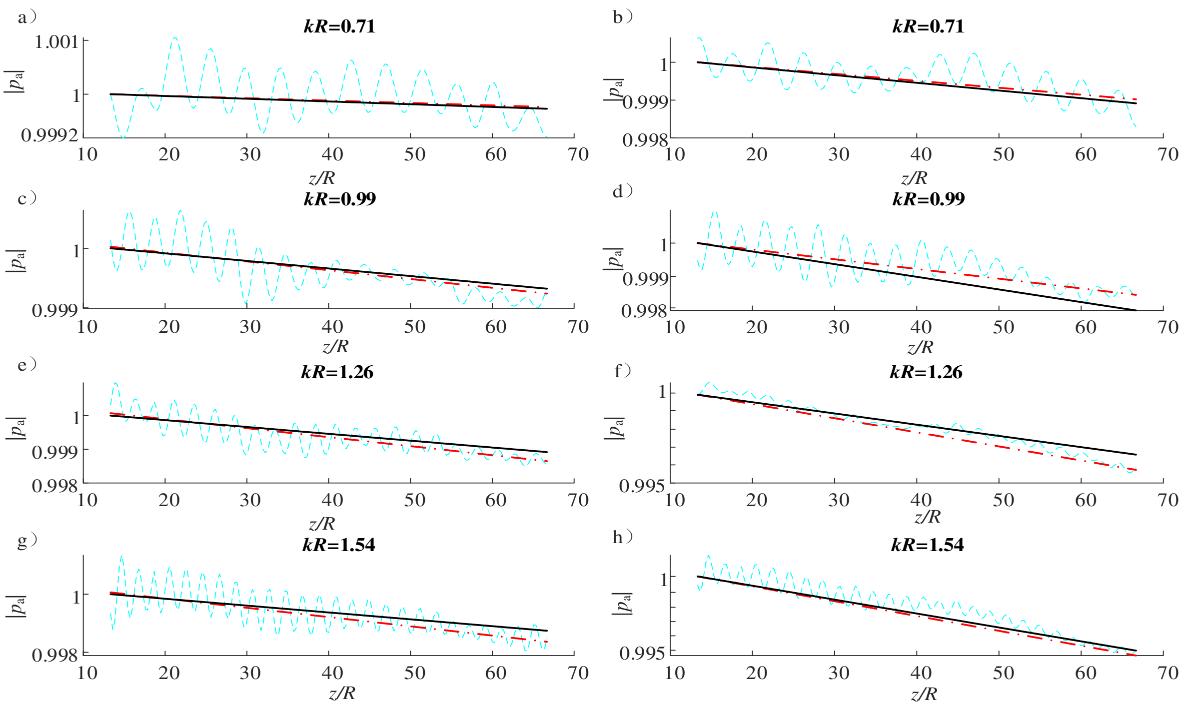

Figure 7. The averaged absolute sound pressure (normalized) varies as a function of the normalized axial distance (z/R) for the plane wave frequency regime ($f < f_{10}$): (left figures (a),(c),(e),(g)) $\sigma/R = 0.05$ and (right figures (b),(d),(f),(h)) $\sigma/R = 0.1$. Cyan dashed lines: averaged absolute pressure from simulation results; red dashed-dotted lines: fitted curve with exponential decay from simulation results; black solid lines: analytical result from Eq. (54).

In Figure 7, the dependence of the averaged acoustic pressure on the distance range along the waveguide is illustrated. To reduce the oscillation in the numerical solution along the distance range, 40 simulation results were predicted and averaged with a moving average filter [16]. Since there still exists the oscillation of the averaged absolute pressure, a curve fitting with the exponential function was used to enable the comparison of the numerical results with the analytical results. A maximum error of 17% between the numerical and analytical solution was observed. This accuracy of the approximation at the end of the distance range is comparable to the results from Ref. [16] when the frequency of the plane wave approaches f_{10}. The numerical simulation was also carried out at higher frequency beyond the first cut-off frequency.

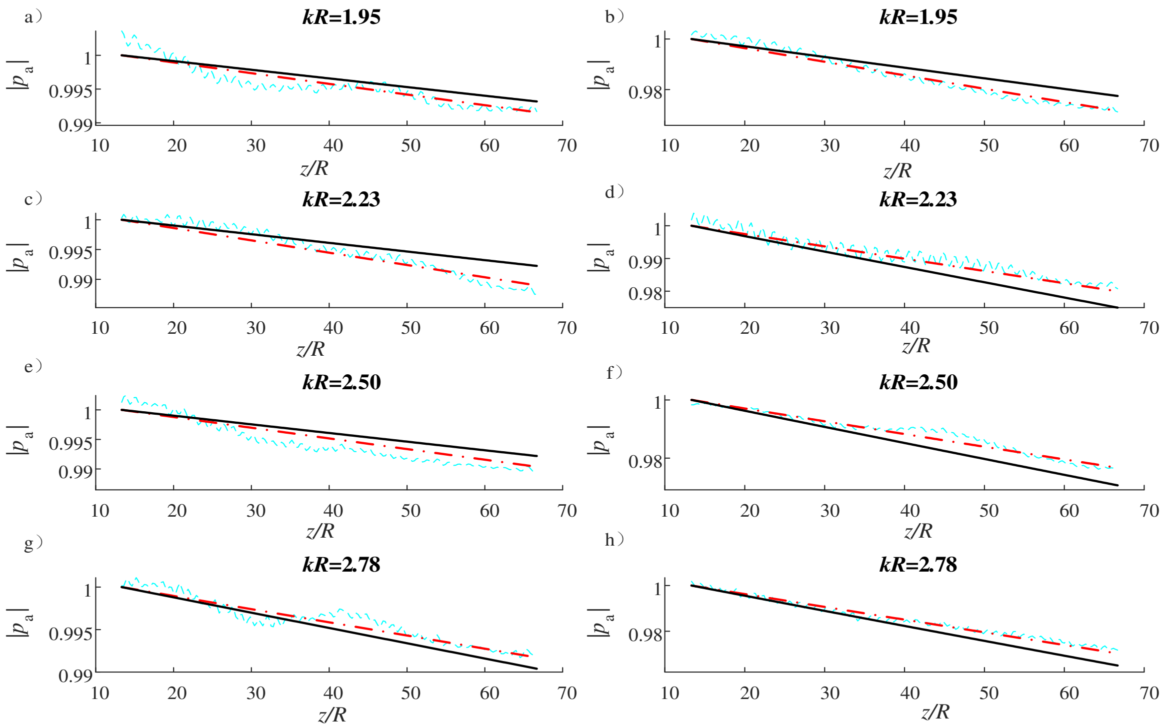

Figure 8. The average absolute sound pressure for the plane wave mode as a function of the normalized axial distance (*z/R*) in the frequency range $f_{10}<f<f_{20}$: (left figures (a),(c),(e),(g)) $\sigma/R = 0.05$ and (right figures (b),(d),(f),(h)) $\sigma/R = 0.1$. Cyan dashed lines: averaged absolute pressure from simulation results; red dashed-dotted lines: fitted curve with exponential decay from simulation results; black solid lines: analytical result from Eq. (57).

In Figure 8, the comparison of the averaged absolute plane wave mode sound pressure between the numerical and analytical results is illustrated in the frequency range $f_{10}<f<f_{20}$. Less than 16% error between the numerical and analytical solution is observed, similar to accuracy of the method illustrated in Figure 7 and also in Ref. A better agreement between the analytical model and the numerical simulation is expected with sufficient realizations of the numerical simulation [16].

The reasonable agreement between the analytical model and the numerical study provides the evidence of the advantage of using this theoretical solution for the estimation of average sound field in the rough waveguide.

C. Wavenumber Correction

This section pertains to the examination of the imaginary component of the wavenumber correction term within the analytical model ($\xi_{00,2}$ in Eqs. (54-58)) under plane wave excitation, wherein a comparative analysis is conducted against the corresponding numerical simulation, as evident from the observed attenuation.

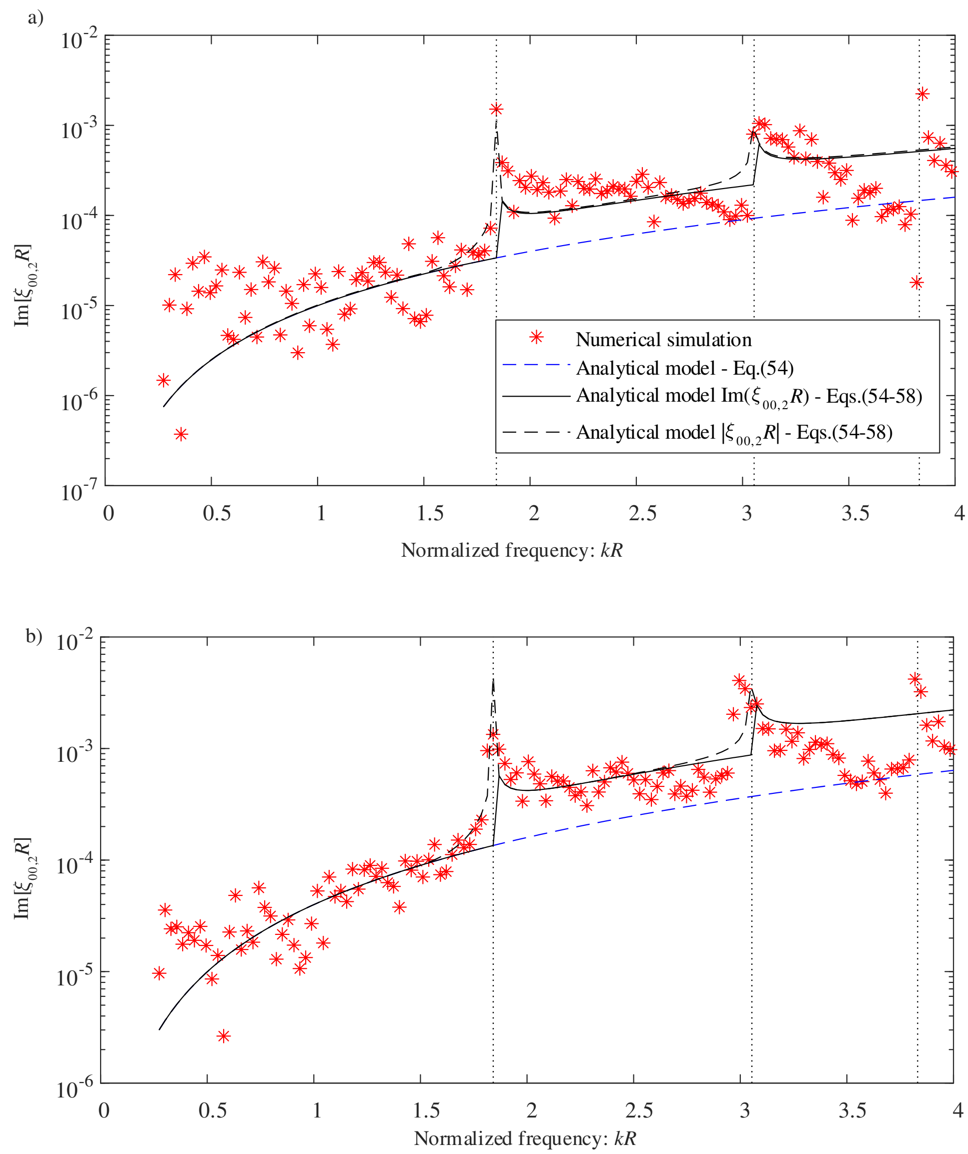

Figure 9. The normalized wavenumber correction $\xi_{00,2}$ as a function of the normalized frequency kR for the plane wave mode: (top) $\sigma/R = 0.05$ and (bottom) $\sigma/R = 0.1$. Red star points: numerical simulation results; dashed lines: analytical mode from Eq. (54) using plane wave without higher modes interference; solid black lines: analytical model using the imaginary part of $\xi_{00,2}R$ from Eq.

(54)-(58) with higher modes interference; dashed black lines: analytical model using the absolute value of $\xi_{00,2}R$ from Eq. (54)-(58) with higher modes interference

Figure 9 shows the comparison of the value of the eigen-value correction predicted with the analytical solution (Eqs. (54)-(58)) and numerical simulation. The numerical counterpart is approximated based on the assumption of exponential decay (Eq. (55)) which can then be defined as [16]:

$$Im[\xi_{00,2}] \approx \frac{1}{|p_{\text{num}}|}\frac{d|p_{\text{num}}|}{dz}, \qquad (59)$$

where $Im[\xi_{00,2}]$ denotes the imaginary part of $\xi_{00,2}$. The wavenumber corrections term from Eqs. (54)-(58) results in higher accuracy capable of recovering the coupled modes effect compared to that when using Eq. (54) only. The accuracy of the numerical results is also expected to deteriorate in the vicinity of the cut-off frequency due to the singular solution. The difference between the imaginary part result and the absolute value of the normalized correction wavenumber indicating the effects from the propagation wave (real wavenumber) at the vicinity frequency range below the cut-off frequencies . These evanescent waves can “propagate” along the pipe due to the continuous scattering from the rough surface which contributes to an real apart of the wavenumber.

IV. Conclusions

This paper discusses the acoustic wave scattering and attenuation in a cylindrical pipe with surface roughness. Based on method developed from the previous study [16] which focuses on a 2-D waveguide, this work derived a theoretical 3-D solution of the averaged plane wave field. Compared with the previous studies, the frequency range of the benchmark analysis has been extended beyond the first two eigen frequencies. The modal coupling between plane wave and first two non-axisymmetric modes is studied analytically. The wave dispersion and the cut-off frequency change due to the roughness have also been studied analytically and numerically. A better understanding the above phenomena is the main novelty of this paper.

Using the SPM and Fourier analysis, this paper derived analytically the averaged components of the wave field. The asymptotic solution of the averaged plane wave field, the corrected plane wave mode wavenumber and the wave dispersion curve shows close agreement with the numerical results obtained with the Monte Carlo method using an FEM Comsol solver. It is noted that computational time of the analytical solution is more than 10^4 times faster compared to that of the numerical solutions. The asymptotic solution can be used to analyse the acoustic wave attenuation in rough cylindrical pipes and in an inverse problem to estimate the pipe roughness from the measured acoustic wave.

Acknowledgement

This work is supported by the UK's Engineering and Physical Sciences Research Council (EPSRC) Programme Grant EP/S016813/1. For the purpose of open access, the author has applied a ‘Creative Commons Attribution (CC BY) licence to any Author Accepted Manuscript version arising. The authors would also like to thank the anonymous reviewers of this paper for constructive comments.

Appendix

This Appendix presents the numerical simulation of the acoustic field distribution in a cylindrical pipe without surface roughness using background plane wave excitation.

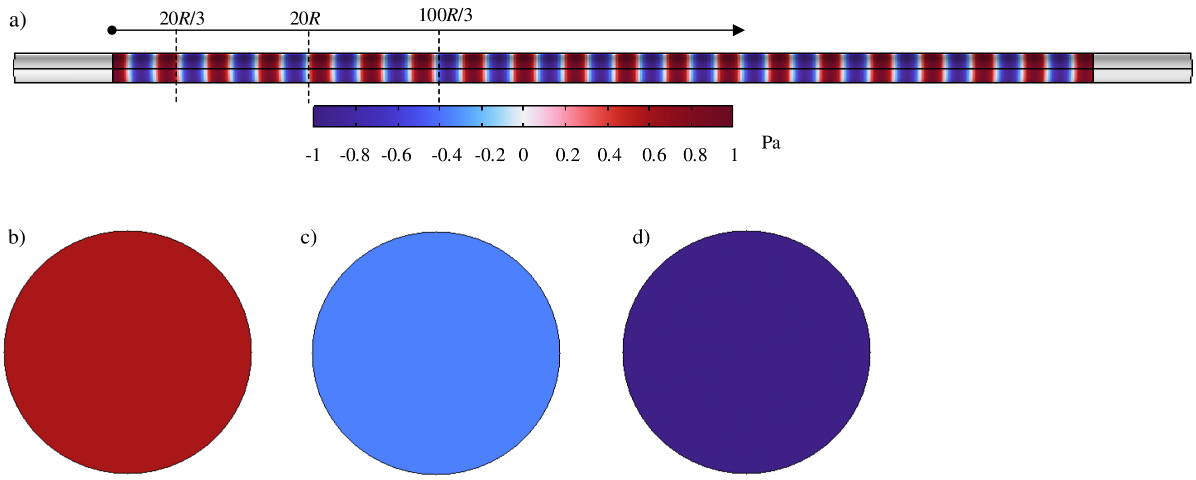

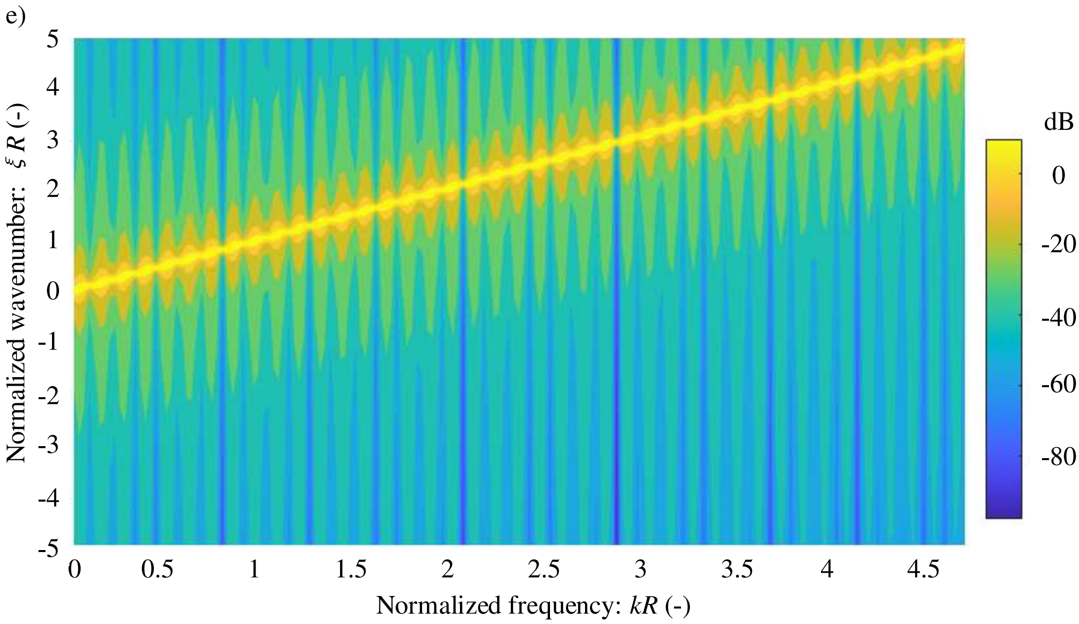

A1 (a) an illustration of the acoustic field distribution (real part) using plane wave background excitation in a pipe without surface roughness at normalized frequency kR=1.81; (b),(c),(d) the cross section acoustic pressure distribution at axial coordinates $20R/3$, $20R$, and $100R/3$, respectively; (e) the dispersion relations of plane wave background excitation in a pipe without surface roughness, Colormap: COMSOL simulation (amplitude of sound pressure). Colour-bar: normalized amplitude of acoustic pressure level (dB).

References

[1] C. C. Mei and M. J. Hancock, "Weakly nonlinear surface waves over a random seabed," *Journal of Fluid Mechanics,* no. 475 , pp. 247-268, 2003.

[2] L. Rayleigh, "On the dynamical theory of gratings," *Proc. R. Soc.,* vol. 79, pp. 399-416, 1907.

[3] E. I. Thorsos and D. R. Jackson, "The validity of the perturbation approximation for rough surface scattering using a Gaussian roughness spectrum," *J. Acoust. Soc. Am,* vol. 86, p. 261–277, 1989.

[4] C. Eftimiu, "Electromagnetic scattering by rough conducting circular cylinders, I: Angular corrugation," *IEEE Trans. Antennas Propag.,* vol. 36, pp. 651-658, 1998.

[5] L. M. Brekhovskikh, "Diffraction of acoustic and electromagnetic waves on wavy surfaces," *J. Exp. Theor. Phys.,* vol. 23, pp. 275-288, 1952.

[6] C. Eckart, "The Scattering of Sound from the Sea Surface," *J. Acoust. Soc. Am,* vol. 25, p. 566–570, 1953.

[7] J. A. Ogilvy, Wave scattering from rough surfaces, Rep. Prog. Phys., 1987.

[8] A. Voronovich, "Small slope approximation in wave scattering theory for rough surfaces.," *Zhurnal Eksp. Teor. Fiz,* vol. 89, p. 116–125, 1985.

[9] M. Collins, "A split-step Padé solution for the parabolic equation method.," *J. Acoust. Soc. Am.,* vol. 93, p. 1736–1742, 1993.

[10] T. M. Elfouhaily and C.-A. Guerin, "A critical survey of approximate scattering wave theories from random rough surfaces," *Waves Random Media,* vol. 14, pp. R1-R40, 2004.

[11] M. Darmon, V. Dorval and F. Baqué, "Acoustic scattering models from rough surfaces: A brief review and recent advances," *Applied Sciences,* vol. 10, p. 22, 2020.

[12] F. G. Bass, V. D. Freulicher and I. M. Fuks, "Propagation in statistically irregular waveguides—Part I: Average field," *IEEE Trans. Antennas Propag.,* vol. 22, pp. 278-288, 1974.

[13] G. A. Maximov, E. V. Podjachev and K. V. Horoshenkov, "Attenuation and scattering of axisymmetrical modes in a fluid-filled round pipe with internally rough walls," *J. Acoust. Soc. Am.,* vol. 123, p. 1248–1259, 2008.

[14] T. Valier-Brasier, C. Potel and M. Bruneau, "On the modeling of modes coupling in dissipative fluid-filled waveguide with corrugated surfaces," *J. Appl. Phys.,* vol. 106, p. 034913, 2009.

[15] A. G. Eguiluz and A. A. Maradudin, "Frequency shift and attenuation length of a Rayleigh wave due to surface roughness," *Physical Review B,* vol. 28, no. 2, p. 728, 1983.

[16] A. Krynkin, K. V. Horoshenkov and S. J. Tait, "An eigenvalue correction due to scattering by a rough wall of an acoustic waveguide," *The Journal of the Acoustical Society of America,* no. 134(2), pp. 939-949, 2013.

[17] A. V. Romanova, K. V. Horoshenkov and A. Krynkin, "Dynamically rough boundary scattering effect on a propagating continuous acoustical wave in a circular pipe with flow," *Sensors,* vol. 18, no. 4, p. 1098, 2018.

[18] Y. Yu, A. Krynkin, Z. Li and K. V. Horoshenkov, "Analytical and empirical models for the acoustic dispersion relations in partially filled water pipes," *Applied Acoustics,* vol. 179, no. 0003-682X, p. 108076, 2021.

[19] "Discover water: treating sewage," 2020. [Online]. Available: https://discoverwater.co.uk/treating-sewage.

[20] T. L. Nguyen, A. Blight, A. Pickering, G. Jackson-Mills, A. R. Barber, J. H. Boyle, R. Richardson, M. Dogar and N. Cohen, "Autonomous control for miniaturized mobile robots in unknown pipe networks," *Frontiers in Robotics and AI,* vol. 9, no. 16, 2022.

[21] Y. Yu, R. Worley, S. Anderson and K. V. Horoshenkov, "Microphone array analysis for

simultaneous condition detection, localization, and classification in a pipe," *The Journal of the Acoustical Society of America,* vol. 153, no. 367 , p. 367–383, 2023.

[22] G. Sarris, S. G. Haslinger, P. Huthwaite, P. B. Nagy and M. J. Lowe, "Attenuation of Rayleigh waves due to surface roughness," *The Journal of the Acoustical Society of America,* vol. 149, no. 6, pp. 4298-4308, 2021.

[23] W. Choi, F. Shi, M. J. Lowe, E. A. Skelton, R. V. Craster and W. L. Daniels, "NDT & E International," *Rough surface reconstruction of real surfaces for numerical simulations of ultrasonic wave scattering,* no. 98, pp. 27-36, 2018.

[24] J. Zhang, B. W. Drinkwater and P. D. Wilcox, "Longitudinal wave scattering from rough crack-like defects.," *IEEE transactions on ultrasonics, ferroelectrics, and frequency control,* vol. 58, no. 10, pp. 2171-2180, 2011.

[25] P. M. Morse and K. U. Ingard, Theoretical acoustics, Princeton university press, 1986.

[26] J. R. Dormand and P. J. Prince, "A family of embedded Runge-Kutta formulae," *J. Comp. Appl. Math.,* vol. 6, p. 19–26, 1980.

[27] Y. Duan and M. McIver, "Rotational acoustic resonances in cylindrical waveguides," *Wave motion,* vol. 39, no. 3, pp. 261-274, 2004.